Journal of Solid State Chemistry **150,** 62–71 (2000)
doi:10.1006/jssc.1999.8548, available online at http://www.idealibrary.com on IDEAL®

Relationship between the Synthesis Conditions and the Structural, Electrical, Magnetic, and Hydrogen Absorption Properties of the Ternary Compounds $GdNi_3X_2$ with X = Al, Ga, or Sn

S. Pechev, J.-L. Bobet, B. Chevalier,[1] B. Darriet, and F. Weill

Institut de Chimie de la Matière Condensée de Bordeaux, ICMCB-CNRS, [UPR 9048], Université Bordeaux I, Avenue du Dr. A. Schweitzer, 33608 Pessac, France

Received July 1, 1999; in revised form October 12, 1999; accepted October 22, 1999

The crystal structure of the ternary compounds $GdNi_3X_2$ (X = Al, Ga, or Sn) obtained by melting (M-sample) and subsequent annealing at 1273 K (A1-sample) or 1073 K (A2-sample) has been investigated by means of X-ray powder diffraction and transmission electron microscopy. $GdNi_3Sn_2$ crystallizes at all temperatures, in the hexagonal $HoNi_{2.6}Ga_{2.4}$-type. $GdNi_3Ga_2$ presents two varieties: the high-temperature form (M-sample) adopts the hexagonal $CaCu_5$-type, whereas the $HoNi_{2.6}Ga_{2.4}$-type is observed for the A2-sample. The structural properties of $GdNi_3Al_2$ (M- and A1-samples) are more complicated; the electron diffraction patterns suggest the occurrence of a new superstructure of the hexagonal $CaCu_5$-type. The study of the electrical and magnetic properties of these compounds shows that $GdNi_3Ga_2$ is ferromagnetic (T_C = 18.0(5) K), $GdNi_3Sn_2$ orders antiferromagnetically (T_N = 19.5(5) K), and $GdNi_3Al_2$ (M- or A1-sample) presents a ferromagnetic behavior (T_C = 20.0(5) K). Moreover, the hydrogen absorption properties of the Al-based intermetallic are dependent on its synthesis conditions. © 2000 Academic Press

Key Words: **gadolinium intermetallics; transmission electron microscopy; magnetism; hydrogenation.**

1. INTRODUCTION

The binary compound $GdNi_5$ orders ferromagnetically below $T_C = 29.3$ K and crystallizes in the hexagonal $CaCu_5$-type structure ($P6/mmm$ space group) (1), Ni-atoms occupying two nonequivalent sites, 2*c* (1/3 2/3 0) and 3*g* (1/2 0 1/2). The structure can be described as a stacking of two atomic planes along the *c*-axis: one at $z = 0$ is formed by Gd (site 1*a* (0 0 0)) and Ni (2*c*)-atoms, whereas the second one located at $z = 1/2$ contains only Ni (3*g*)-species. The substitution of an X *p*-element such as Al, Ga, or Sn for Ni involves, versus composition range, a structural transition in the $GdNi_{5-x}X_x$ systems (2–5). For instance, the ternary compounds $GdNi_3Ga_2$ and $GdNi_3Sn_2$ adopt the hexagonal $HoNi_{2.6}Ga_{2.4}$-type structure ($P6/mmm$ space group) (6), which derives from the $CaCu_5$-type. The unit cell parameters of these two structures are related as follows: $a_{HoNi_{2.6}Ga_{2.4}} = a_{CaCu_5}\sqrt{3}$, and $c_{HoNi_{2.6}Ga_{2.4}} = c_{CaCu_5}$. A representation of these two crystallographic structures is given in detail in Refs. (2, 4, 5). The occurrence of the $HoNi_{2.6}Ga_{2.4}$-type is connected with a steric effect: the substitution of a larger X-element for Ni leads to a shift of some of the Gd-atoms along the *c*-axis to the $z = 1/2$ plane. In this structure type, Gd-atoms occupy two sites, 1*a* (0 0 0) and 2*d* (1/3 2/3 1/2), whereas Ni species are located, for instance in $GdNi_3Sn_2$ (3), on the 6*l*-site ((0.178 0.356 0); 100% occupancy) and on the 3*f*-site (1/2 0 0) and 6*k*-site (0.272 0 1/2) (statistically distributed with Sn). Here, the Gd-atoms are distributed on the two atomic planes perpendicular to the *c*-axis at $z = 0$ and 1/2.

Recently we have shown that the solid solutions $GdNi_{5-x}Al_x$, obtained by melting and subsequent annealing at 1073 K, exhibit the compositional structural transition described above: the alloys with $0 \le x \le 1.74$ crystallize in the hexagonal $CaCu_5$-type, whereas for $2.01 \le x \le 3.07$ a larger hexagonal unit cell of the $HoNi_{2.6}Ga_{2.4}$-type is observed (5). A decrease of the hydrogen absorption properties of these intermetallics accompanies the structural change since a drastic decrease of the maximum hydrogen content (2.6(1) → 1.3(1)), in number of H-atoms ($GdNi_{5-x}Al_x$ formula unit), appears for x of about 1.7 to 2 (5).

In order to extend our knowledge of this system, we have prepared $GdNi_3Al_2$ with different heat treatments with melting only or additional annealing, respectively, at 1273 and 1073 K, and studied the influence of the annealing on its structural properties. In this paper, we discuss these properties, investigated by means of both X-ray powder diffraction and electron transmission microscopy and compare them with those of $GdNi_3Ga_2$ and $GdNi_3Sn_2$ obtained by the

[1]To whom correspondence should be addressed. Fax: 33-5-56842761. E-mail: chevalie@icmcb.u-bordeaux.fr.

0022-4596/00 $35.00

same routes. The electrical and magnetic properties of these three intermetallics are also presented. Moreover the hydrogen absorption properties of $GdNi_3Al_2$ are investigated.

2. EXPERIMENTAL DETAILS

The samples $GdNi_3X_2$ (X = Al, Ga, or Sn) were synthesized by arc-melting a stoichiometric mixture of pure elements in an argon atmosphere. They were remelted four times in order to ensure their homogeneity then divided into three parts: one (M) was kept after melting, and the two other were vacuum annealed, respectively, at 1273 (A1) and 1073 K (A2) for one month. The phase purity of each sample was checked by electron microprobe analysis with a CAMECA SX-100 instrument. The determination of the chemical composition of the various phases was performed on the basis of intensity measurements of $GdL\alpha_1$, $NiK\alpha_1$, $AlK\alpha_1$, $GaL\alpha_1$, and $SnL\alpha_1$ X-ray emission lines, which were compared with those obtained for Gd_2Ni_2X (X = Al, Ga, or Sn) used as reference compounds. The samples were characterized by X-ray powder diffraction (Guinier camera, $CuK\alpha_1$ radiation). The lattice parameters were determined by a least-squares refinement method using 5 N silicon ($a = 0.54307$ nm) as internal standard.

For the investigations with a transmission electron microscope (JEOL 2000FX), parts of the samples were crushed in ethanol, and the small crystal fragments were placed on a copper grid covered with an amorphous holey carbon film.

Hydrogen absorption measurements were performed at room temperature using the apparatus and the procedure described previously (5). Magnetizations of the initial and the hydrogenated samples were determined between 4.2 and 300 K in fields up to 5 T using a SQUID magnetometer. Electrical resistivity measurements were carried out by a standard four-probe dc-technique in the range 4.2–290 K.

3. RESULTS AND DISCUSSION

3.1. Microprobe Analysis

Table 1 summarizes the chemical analysis of the three intermetallics $GdNi_3X_2$ (X = Al, Ga, or Sn) obtained under the different heat treatment conditions.

Concerning $GdNi_3Al_2$, this analysis shows that M- and A1-samples are practically a single phase, having, respectively, $GdNi_{3.10(4)}Al_{1.90(4)}$ and $GdNi_{3.05(2)}Al_{1.95(2)}$ chemical compositions. The first one contains Gd_2Ni_2Al and NiAl as impurities phases (< 3–4% in mass) while the second one contains only some traces of NiAl. The A2-sample is a mixture of two compositions, $GdNi_{3.10(2)}Al_{1.90(2)}$ and $GdNi_{2.97(1)}Al_{2.03(1)}$, showing the thermal instability of this intermetallic. It is interesting to note that the chemical composition of the A1-sample ($GdNi_{3.05(2)}Al_{1.95(2)}$) is intermediate between those found in A2; confirming the decomposition of this Al-based intermetallic at 1073 K.

TABLE 1
Chemical Composition, Determined by Microprobe Analysis, of the Samples $GdNi_3X_2$ (X = Al, Ga, or Sn)

Sample	Thermal treatment	Microprobe analysis	
		Major phase	Impurities phases
$GdNi_3Al_2$	M	$GdNi_{3.10(4)}Al_{1.90(4)}$	Gd_2Ni_2Al, NiAl
	A1	$GdNi_{3.05(2)}Al_{1.95(2)}$	NiAl
	A2	$GdNi_{3.10(2)}Al_{1.90(2)}$	NiAl
		$GdNi_{2.97(1)}Al_{2.03(1)}$	
$GdNi_3Ga_2$	M	$GdNi_{3.01(1)}Ga_{1.99(1)}$	none
	A1	$GdNi_{2.98(1)}Ga_{2.02(1)}$	NiGa
	A2	$GdNi_{2.99(1)}Ga_{2.01(1)}$	none
$GdNi_3Sn_2$	M	$GdNi_{3.01(1)}Sn_{1.99(1)}$	$GdNi_2Sn_2$, Ni_3Sn_2
	A1	$GdNi_{2.99(1)}Sn_{2.01(1)}$	Ni_3Sn_2
	A2	$GdNi_{3.01(3)}Sn_{1.99(4)}$	Ni_3Sn_2

Note. "M" indicates obtained by melting only and "A1" or "A2" indicates after additional annealing at 1273 or 1073 K, respectively.

The analysis performed on $GdNi_3Ga_2$ and $GdNi_3Sn_2$ does not reveal a similar decomposition of the A2-samples. $GdNi_3Ga_2$ is obtained as a single phase after melting (M) or after additional annealing at 1073 K (A2); some traces of equiatomic binary gallide NiGa are detected in the A1-sample. It is difficult to prepare the ternary stannide $GdNi_3Sn_2$ without any impurities; for instance Ni_3Sn_2 (< 2% in mass) is still present in the different samples.

3.2. X-Ray Powder Diffraction and Transmission Electron Microscopy

3.2.1. X-Ray Powder Diffraction Patterns

The X-ray powder pattern of $GdNi_3Sn_2$ obtained by melting (M) or after additional annealing (A1, A2) can be completely indexed with a hexagonal unit cell having the structure type $HoNi_{2.6}Ga_{2.4}$ (Table 2). The lattice parameters are comparable to those determined previously (3).

The structural properties of $GdNi_3Ga_2$ are dependent on the sample preparation procedures: obtained by melting and quenching (M-sample), it adopts the hexagonal $CaCu_5$-type, but after an annealing at 1073 K (A2-sample) it adopts the $HoNi_{2.6}Ga_{2.4}$-type (Table 2). These results indicate that $GdNi_3Ga_2$ has two polymorphic forms: the high temperature one is reported here for the first time. It is interesting to note that the A1-sample, mainly constituted by one single ternary chemical composition (Table 1), contains these two polymorphic forms (Table 2). So we may conclude that the structural transition $CaCu_5$-type → $HoNi_{2.6}Ga_{2.4}$-type appears for this ternary gallide around

TABLE 2
Crystallographic (V_m = Unit Cell Volume) and Magnetic Data Relative to the Ternary Compounds $GdNi_3X_2$ (X = Al, Ga, or Sn)

Sample	Thermal treatment	Type structure	Crystallographic data			Magnetic data			Ref.
			a (nm)	c (nm)	V_m (nm)^3	$\mu_{eff.}$ (μ_B/Gd)	θ_p (K)	T_{mag} (K)	
$GdNi_3Al_2$	M	unknown	0.8762(1)	0.8126(2)	0.54027(8)	8.53(10)	18(1)	$T_C = 20.0(5)$	this work
	A1	unknown	0.8761(2)	0.8158(2)	0.54228(12)	8.16(10)	18(1)	$T_C = 20.0(5)$	this work
	A2	unknown	0.8768(1)	0.8156(1)	0.54301(6)	8.27(10)	14(1)	$T_C = 20.4(5)$	this work
		$HoNi_{2.6}Ga_{2.4}$	0.8769(2)	0.4113(2)	0.27390(9)			$T_1 = 11.1(5)$; $T_2 = 3.9(5)$	
	ann. 1100 K	$CaCu_5$	0.5067	0.4083	0.09078				(4)
$GdNi_3Ga_2$	M	$CaCu_5$	0.5086(8)	0.4051(1)	0.09075(30)	8.36(10)	15(1)	$T_C = 17.5(5)$	this work
	A1	$CaCu_5$	0.5070(4)	0.4052(3)	0.09020(21)				this work
		$HoNi_{2.6}Ga_{2.4}$	0.8717(8)	0.4131(5)	0.27184(28)				
	A2	$HoNi_{2.6}Ga_{2.4}$	0.8737(1)	0.4132(1)	0.27316(4)	8.09(10)	16(1)	$T_C = 18.0(5)$	this work
	A1	$HoNi_{2.6}Ga_{2.4}$	0.8748	0.4111	0.27246				(2)
$GdNi_3Sn_2$	M, A1, A2	$HoNi_{2.6}Ga_{2.4}$	0.9175(1)	0.4259(1)	0.31049(5)	8.23(10)	−17(1)	$T_N = 19.5(5)$	this work
		$HoNi_{2.6}Ga_{2.4}$	0.9207	0.4280	0.31420	8.0	−9		(3)

1273 K. Since the date our work was submitted, similar results were reported by Blazina *et al.* (7).

The examination of the X-ray powder diffraction pattern of $GdNi_3Al_2$ (A1-sample) indicates (Fig. 1): (i) that the major peaks can be indexed on the basis of a hexagonal unit cell having $CaCu_5$-type with parameters $a = 0.5058(2)$ nm and $c = 0.4079(2)$ nm; (ii) the presence of cubic NiAl (8) as an impurity phase in agreement with the results obtained by microprobe analysis (Table 1); and (iii) the occurrence of weak reflections near $2\theta = 15.9°$ and 25.8° which could not be indexed with the hexagonal $CaCu_5$ or with the $HoNi_{2.6}Ga_{2.4}$ unit cell. The additional reflections suggest that the crystal structure of this compound is not a simple $CaCu_5$-type. Similar comments can be made concerning the X-ray powder diffraction pattern of the M-sample of this intermetallic. The investigation of the A2-sample reveals the presence of two majority phases, one adopting the hexagonal-type similar to that observed in the M- or A1-sample and the second the $HoNi_{2.6}Ga_{2.4}$-type with the unit cell parameters as indicated in Table 2. In this case also, additional peaks are detected at $2\theta = 15.9°$ and 25.8°. We recall that this sample contains two ternary compositions (Table 1); perhaps the occurrence of the phase crystallizing with the $HoNi_{2.6}Ga_{2.4}$-type gives evidence of the presence of the aluminum-rich ternary compound $GdNi_{2.97(1)}Al_{2.03(1)}$. Unlike $GdNi_3Ga_2$, the existence of two polymorphic forms for the Al-based intermetallic is ambiguous.

In order to obtain more information concerning $GdNi_3Al_2$, we have investigated its crystal structure by transmission electron microscopy. The results are analyzed in comparison with those obtained for the two polymorphic forms of $GdNi_3Ga_2$. Unfortunately, in spite of our attempt, no single crystal of $GdNi_3Al_2$ has been obtained in order to determine its structural properties by X-ray diffractometry.

3.2.2. *Transmission Electron Microscopy (TEM)*

$GdNi_3Ga_2$. In the TEM investigation, the most significant diffraction patterns of $GdNi_3Ga_2$ (M-sample) are those along the [001] and [0$\bar{1}$0]-zone axis. The selection area electron diffraction pattern (SAED) along the [001]-zone axis (Fig. 2a) consists of a hexagonal arrangement (a = 0.5086 nm) of spots. On the SAED pattern along the [0$\bar{1}$0]-zone axis (Fig. 2b) the reflections are indexed with the unit-cell parameters $a = 0.5086$ nm and $c = 0.4051$ nm corresponding to the hexagonal $CaCu_5$-type structure. For $GdNi_3Ga_2$ (A2-sample), on the SAED patterns (Fig. 3) along the [001] and [0$\bar{1}$0] directions, the spots are

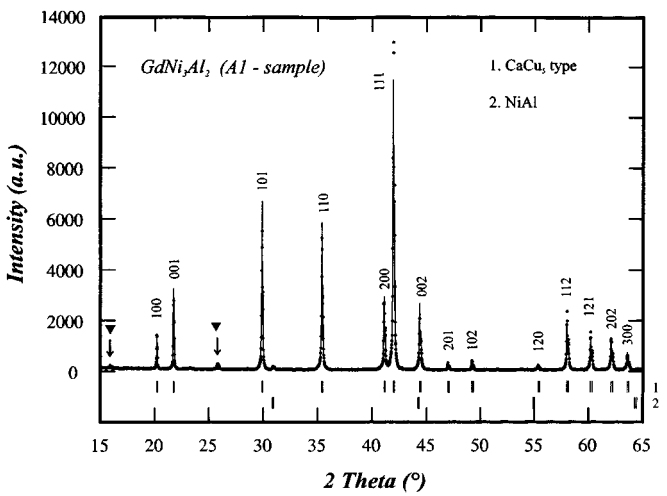

FIG. 1. X-ray powder diffraction pattern of $GdNi_3Al_2$ (A1-sample). The vertical ticks labelled 1 and 2 are, respectively, relative to the $CaCu_5$-type phase ((*hkl*) indices are given) and NiAl. The additional peaks are indicated by the symbol ▼.

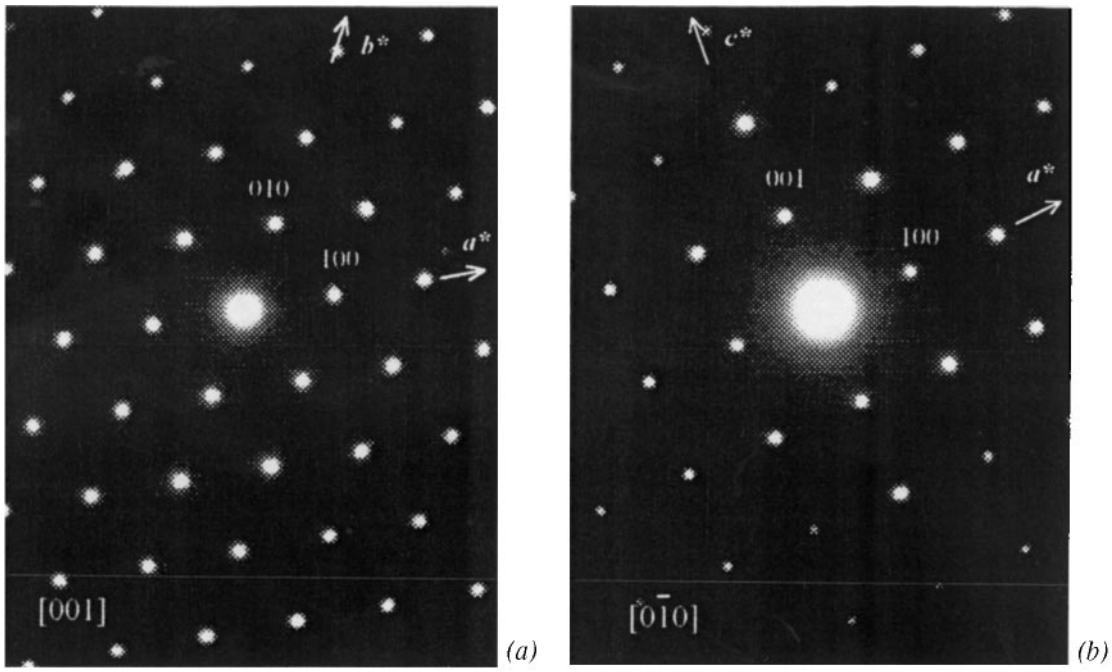

FIG. 2. Electron diffraction patterns of $GdNi_3Ga_2$ (M-sample) along the [001] (a) and the [0$\bar{1}$0] (b) zone axes. Indexation is given on the basis of the $CaCu_5$-type ($a = 0.5086$ nm and $c = 0.4051$ nm).

compatible with a hexagonal unit cell ($a = 0.8737$ nm and $c = 0.4132$ nm) having the structure type $HoNi_{2.6}Ga_{2.4}$.

$GdNi_3Al_2$. The examination of several SAED patterns corresponding to the A1-sample reveals that: (i) the [001]-zone (Fig. 4a) exhibits some similarities to those observed for $GdNi_3Ga_2$ (A2-sample) (Fig. 3a) in that all the spots form a hexagonal array with $a = 0.8761$ nm; (ii) for the [0$\bar{1}$0]-zone (Fig. 4b) an extra row of spots orthogonal to the c*-direction appears compared to the equivalent SAED pattern of $GdNi_3Ga_2$ (A2-sample) (Fig. 3b); (iii) in addition,

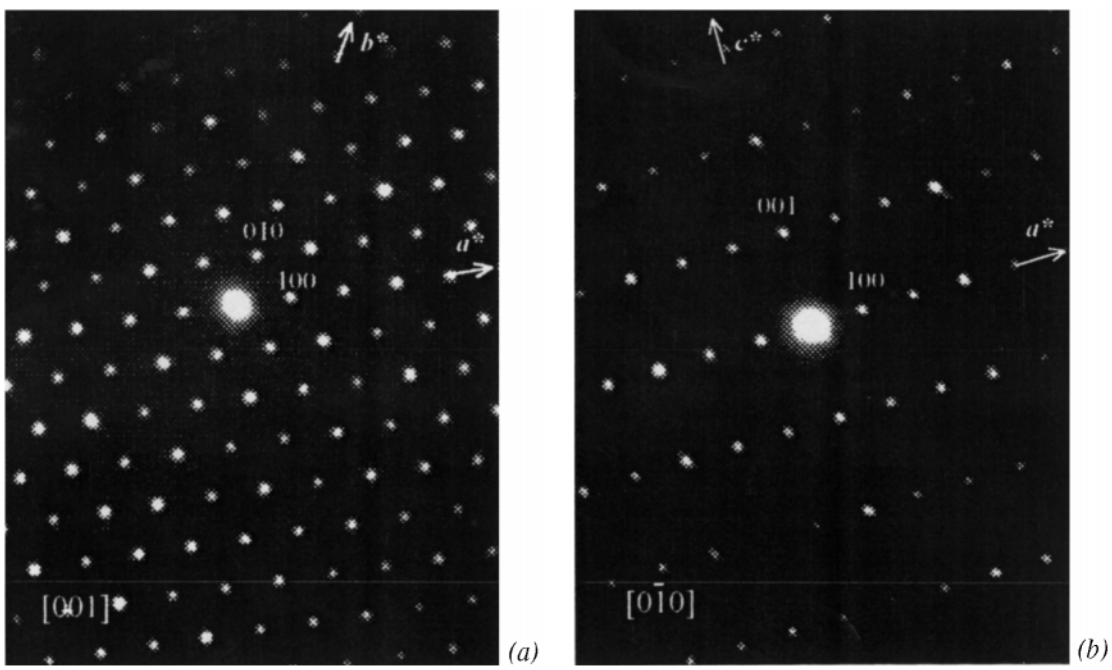

FIG. 3. Electron diffraction patterns of $GdNi_3Ga_2$ (A2-sample) along the [001] (a) and the [0$\bar{1}$0] (b) zone axes. Indexation is given on the basis of the $HoNi_{2.6}Ga_{2.4}$-type ($a = 0.8737$ nm and $c = 0.4132$ nm).

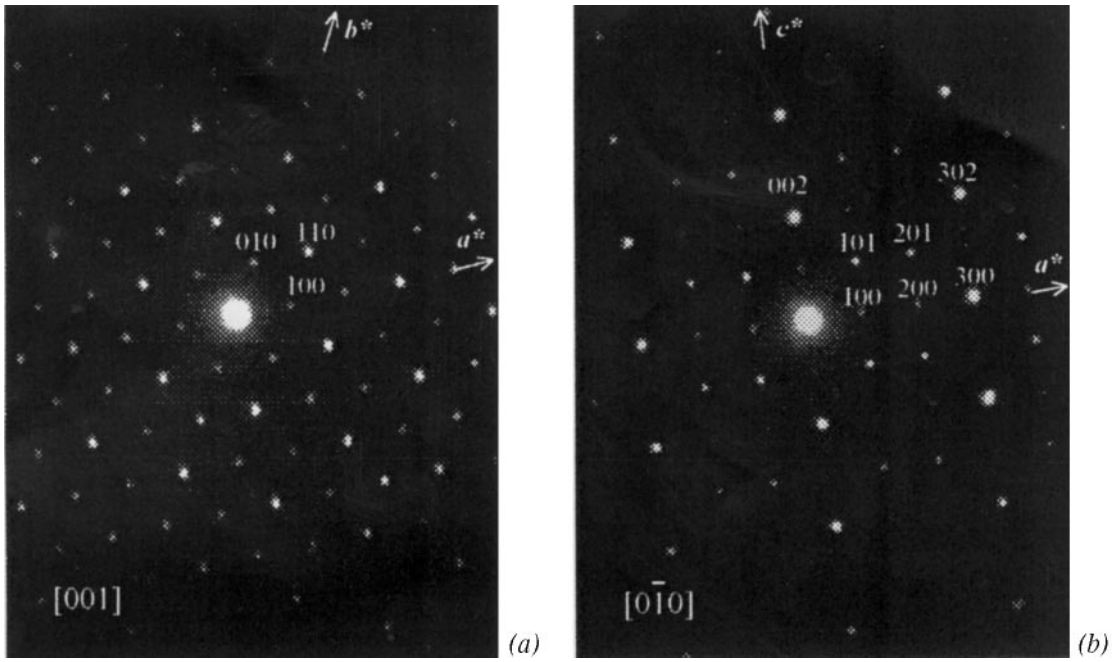

FIG. 4. Electron diffraction patterns of $GdNi_3Al_2$ (A1-sample) along the [001] (a) and the [0$\bar{1}$0] (b) zone axes. Indexation is given on the basis of a hexagonal unit cell ($a = 0.8761$nm and $c = 0.8158$ nm).

the comparison of the spot intensities reveals very important differences between some of them. The hexagonal unit cell corresponding to this unknown-type has $a = 0.8761$ nm and $c = 0.8158$ nm as parameters. We observe the following metric relation to the $CaCu_5$-type and $HoNi_{2.6}Ga_{2.4}$-type: $a = a_{CaCu_5}\sqrt{3} = a_{HoNi_{2.6}Ga_{2.4}}$ and $c = 2c_{CaCu_5} = 2c_{HoNi_{2.6}Ga_{2.4}}$. Considering this result, the small reflections observed at $2\theta = 15.9^\circ$ and 25.8° (Fig. 1) can be indexed as 101 and 201 peaks.

Remark. For $GdNi_3Al_2$ (A1-sample), if we take into account the very important differences between the spot intensities of the SAED pattern, we can suggest another description for the unit cell. We can describe this structure as a superstructure of the $CaCu_5$-type with the unit cell parameters $a = 0.5058$ nm and $c = 0.4079$ nm and the commensurate modulation vector $\mathbf{q} = \frac{1}{3}\mathbf{a}^* + \frac{1}{3}\mathbf{b}^* + \frac{1}{2}\mathbf{c}^*$. With this description the symbol of the (3 + 1) dimensional Bravais class is $6/mmm\ P(1/3\ 1/3\ 1/2)$).

Two crystalline phases have been identified by electron diffraction on $GdNi_3Al_2$ (A2-sample): one of them is the unknown structure noticed in the M- or A1-sample while a hexagonal structure having the $HoNi_{2.6}Ga_{2.4}$-type has been observed for the second one (Table 2).

3.2.3. Discussion of the Structural Properties of $GdNi_3X_2$ ($X = Al$, Ga, or Sn) Compounds

Our results allow us to make several comments about the evolution of the structural properties of these intermetallics.

For Al-based compounds the observed structural transition hexagonal unknown-type → $HoNi_{2.6}Ga_{2.4}$-type could correspond to the existence of two ternary compositions identified in the A2-sample. Each of these two compositions situated on both sides of the stoichiometric $GdNi_3Al_2$ composition (Table 1) could be associated to one of these two structural types. Only a structural determination performed on a single crystal could confirm this hypothesis.

For $GdNi_3Ga_2$ (A1-sample) both the high-temperature form ($CaCu_5$-type) and the low-temperature one ($HoNi_{2.6}Ga_{2.4}$-type) coexist. Each of them has been obtained in the M- and A2-samples, respectively.

On the other hand, the $CaCu_5$-type has never been observed for $GdNi_3Sn_2$.

This result can be explained from the interatomic distances calculated in $GdNi_3Ga_2$ (M-sample). In the $CaCu_5$-type unit cell of this compound (Ni in the 2*c*-site (1/3 2/3 0) and (1/3 Ni + 2/3 Ga) in the 3*g*-site (1/2 0 1/2), the interatomic Ni–Ga (0.2502 and 0.2543 nm) and especially the Ga–Ga (0.2543 nm) distances are shorter than the sum of the atomic radii ($r_{Ni} = 0.1246$ nm and $r_{Ga} = 0.141$ nm). This result suggests that the compounds $GdNi_3Al_2$ and $GdNi_3Sn_2$ with the $CaCu_5$-type structure cannot exist since the aluminum-atom ($r_{Al} = 0.143$ nm) and tin-atom ($r_{Sn} = 0.1623$ nm) are larger than those of gallium.

3.3. Electrical Resistivity and Magnetization Measurements

The binary compounds NiAl, NiGa, and Ni_3Sn_2 detected as impurity phases in the sample are, respectively, Pauli

paramagnets (NiAl and NiGa) (9) and a ferromagnet below 5 K (Ni_3Sn_2) (10).

3.3.1. $GdNi_3Ga_2$

The thermal dependence of the reduced electrical resistivity $\rho(T)/\rho(230\text{ K})$ of $GdNi_3Ga_2$ (M- and A2-samples) is shown in Fig. 5. (Owing to the presence of microcracks in the polycrystalline samples, absolute values of $\rho(T)$ could not be determined accurately; for this reason, reduced resistivity is reported.) In the temperature range 230–25 K, the reduced resistivity of these two samples decreases with temperature, but more rapidly for the A2-sample. The difference in these behaviors could be due to the structural transition $CaCu_5$-type $\rightarrow HoNi_{2.6}Ga_{2.4}$-type and to the annealing treatment which reduces the mechanical stress. A sudden change of slope is detected at 18 and 19 K on the reduced resistivity curves of these two samples, suggesting the occurrence of a magnetic transition. Above this temperature, the resistivity increases continuously but deviates from the linear temperature dependence which characterizes the normal metals. This deviation observed in many compounds based on rare earth elements (11) is attributed to their high value of the resistivity; the mean free path is short, of the order of a few interatomic distances.

Above 25 K, the magnetic susceptibility of this gallide follows a Curie–Weiss law having a positive paramagnetic Curie temperature θ_p (Table 2) which indicates the predominance of the ferromagnetic interactions. The thermal dependence of the magnetization of M- and A2-samples, measured in low-field $B = 0.025$ T, is characteristic of ferromagnetic behavior (Fig. 6). The Curie temperature T_C determined from the inflection point of the curve is equal to 17.5(5) and 18.0(5) K for the M- and A2-samples, respectively. The magnetic properties of $GdNi_3Ga_2$ are then negligibly on their structural properties. At 5 K, the magnetization of the A2-sample takes a value of 7.3(1) μ_B/mol in $B = 4.8$ T (Fig. 7). This value is close to the expected one (7 μ_B) for a Gd^{3+} ion. Previous investigation of $GdNi_3Ga_2$ reported a ferromagnetic behavior without indication of the T_C-temperature (12).

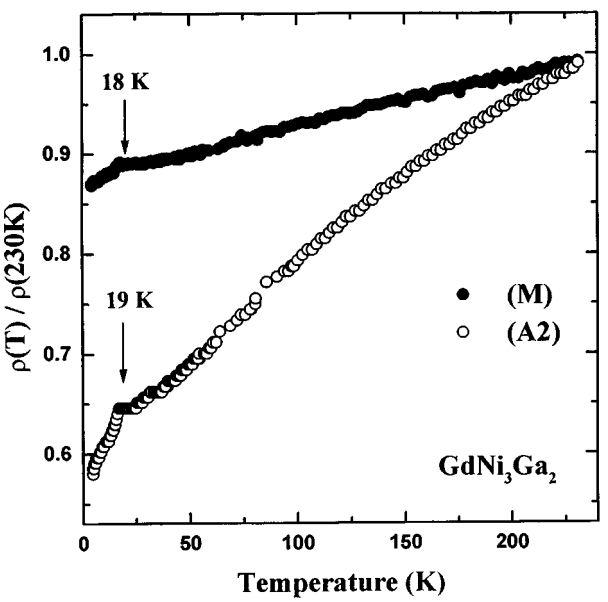

FIG. 5. Thermal dependence of the reduced electrical resistivity of $GdNi_3Ga_2$ (M- and A2-samples).

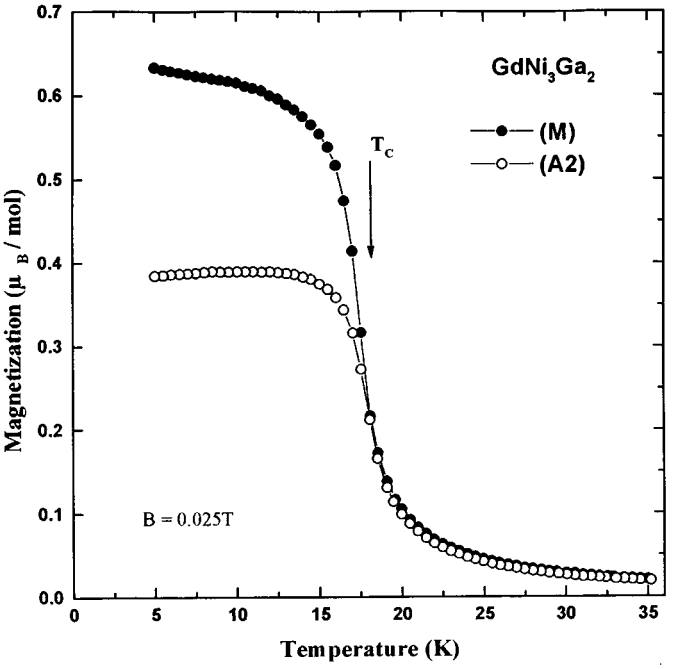

FIG. 6. Temperature dependence of the magnetization of $GdNi_3Ga_2$ (M- and A2-samples) measured with a magnetic field $B = 0.025$ T.

3.3.2. $GdNi_3Sn_2$

The magnetization versus temperature curve of $GdNi_3Sn_2$ (A2-sample), measured in field $B = 0.025$ T, exhibits a shoulder at $T_N = 19.5(5)$ K (Fig. 8) (the increase of magnetization occurring below T_N can be attributed to traces of Ni_3Sn_2 detected by microprobe analysis). This behavior, together with an abrupt decrease of the resistivity in this temperature range (13), indicates that this ternary stannide is magnetically ordered. Below T_N, its magnetization varies linearly with the field (Fig. 7), suggesting an antiferromagnetic type of ordering. This result agrees with the negative value of its Curie paramagnetic temperature $\theta_p = -17$ K (Table 2).

3.3.3. $GdNi_3Al_2$

The thermal dependence of the reduced resistivity of $GdNi_3Al_2$ is given in Fig. 9. The observed behavior is

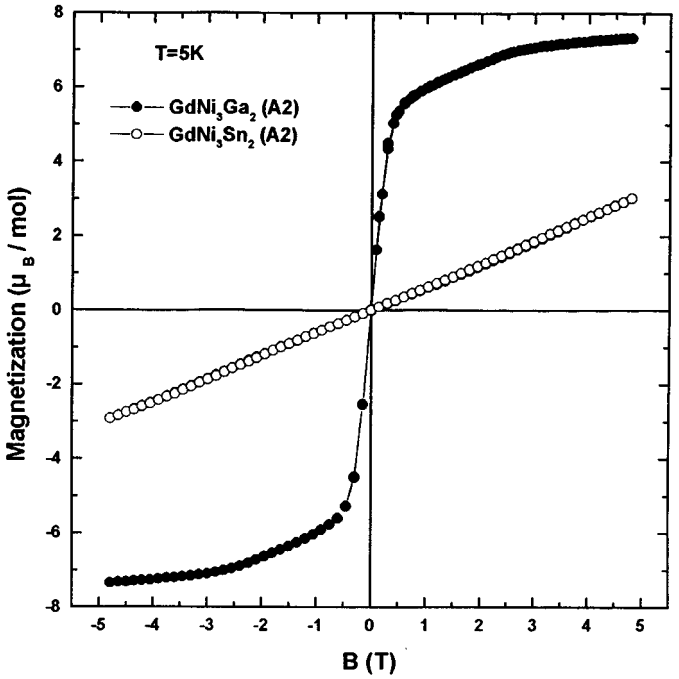

FIG. 7. Field dependence at 5 K of the magnetization of $GdNi_3Ga_2$ and $GdNi_3Sn_2$ (A2-samples).

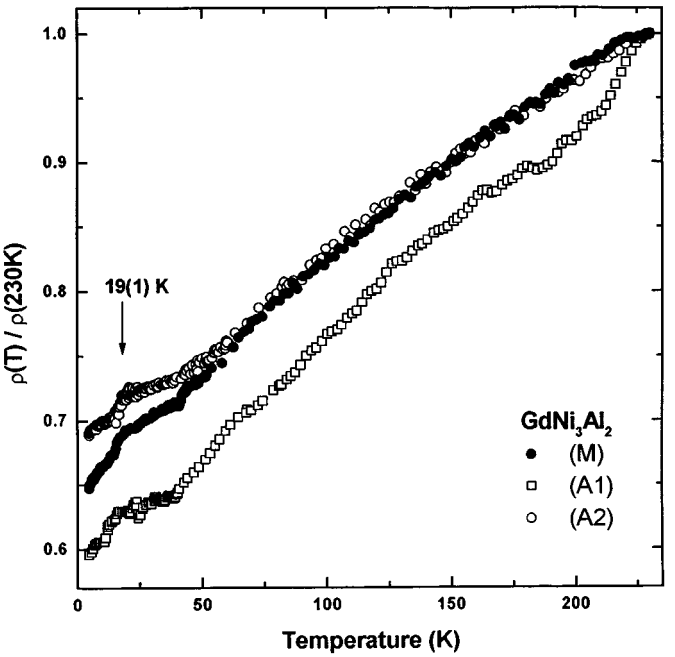

FIG. 9. Thermal dependence of the reduced electrical resistivity of $GdNi_3Al_2$ (M-, A1-, and A2-samples).

dependent on the thermal treatment of the compound: (i) the reduced resistivity of the A1-sample decreases more rapidly than that of the M-sample, confirming that annealing at 1273 K reduces the mechanical stress induced by the melting process; (ii) the reduced resistivity of the A2-sample decreases more weakly with temperature because it is mainly constituted by two ternary alloys (Table 1). But in all cases, a slight slope change of the thermal dependence is observed below 19(1) K, suggesting a decrease of the spin disorder accompanying a magnetic transition.

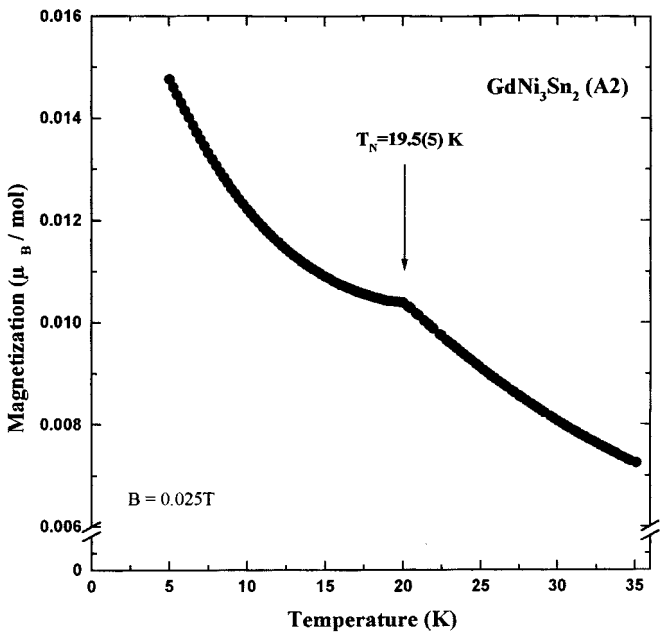

FIG. 8. Thermal dependence of the magnetization of $GdNi_3Sn_2$ (A2-sample) measured with a magnetic field $B = 0.025$ T

In field $B = 0.025$ T, the magnetization of the M- and A1-samples increases rapidly around $T_C = 20.0(5)$ K, indicating the occurrence of a ferromagnetic ordering (Fig. 10). We observe for both samples a positive paramagnetic Curie temperature θ_p (Table 2). The smaller magnetization of the A2-sample shows three anomalies, an increase around $T_C = 20.4(5)$ K and two kinks appearing at $T_1 = 11.1(5)$ K and $T_2 = 3.9(5)$ K (Fig. 10). As the sample is a mixture of two phases, we could ascribe the ferromagnetic transition (T_C) to the phase adopting the unknown hexagonal-type and the two other transitions (T_1 and T_2) to the second phase crystallizing in the $HoNi_{2.6}Ga_{2.4}$-type. This last behavior suggests a change of the magnetic structure in the ordered state as observed in other Al-based intermetallics such as GdNiAl (16).

We have also measured the magnetization of these three samples at 5 K and in magnetic fields up to 4.8 T (Fig. 11). The curve relative to the A1-sample shows a tendency toward saturation with a moment of 7.15(5) μ_B/mol, close to that calculated for a Gd^{3+} ion (7.0 μ_B). The values obtained for the M- and A2-samples are smaller because in one case the sample contains a greater amount of impurity

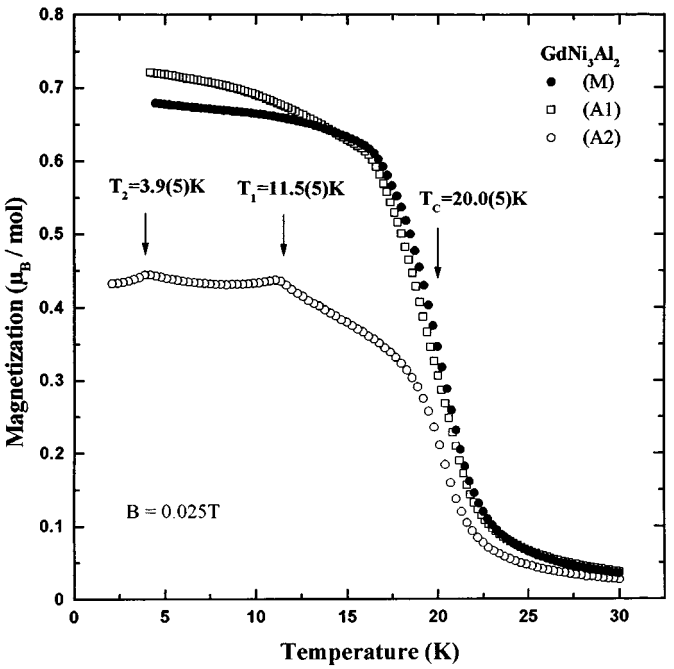

FIG. 10. Temperature dependence of the magnetization, measured with a magnetic field $B = 0.025$ T, of the three $GdNi_3Al_2$ samples.

(M-sample) (Table 1) and in the other case two phases are present (A2-sample). In all cases, no remanence is detected, in agreement with the isotropic character of the Gd^{3+} ion.

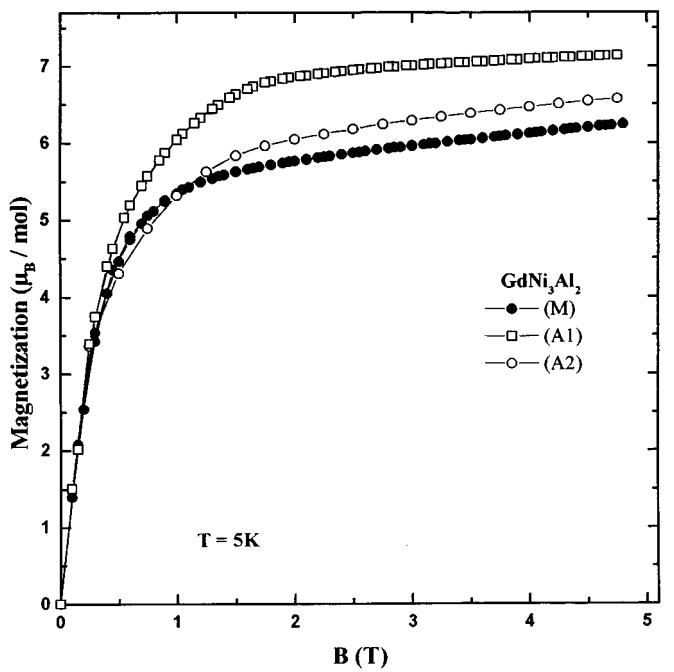

FIG. 11. Field dependence of the magnetization, measured at $T = 5$ K, of the three $GdNi_3Al_2$ samples.

3.3.4. Discussion of the Structural and Magnetic Properties of $GdNi_3X_2$ Compounds

Considering the compounds which adopt the $CaCu_5$-type, we observe a decrease of the Curie temperature T_C following the sequence $GdNi_5$ ($T_C = 29.3$ K) (1) → $GdNi_3Ga_2$ (M-sample; $T_C = 17.5(5)$ K). Such a tendency can be related to the increase of the interatomic Gd–Gd distance. In this structure type, each Gd-atom has eight nearest neighbors, two along the *c*-axis and six in the basal (*a*, *b*)-plane. In the considered compound sequence, the average Gd–Gd distance increases from 0.467 to 0.483 nm for $GdNi_5$ and $GdNi_3Ga_2$, respectively. This fact leads to a enfeeblement of the ferromagnetic interaction taking into consideration the RKKY (Rudermann–Kittel– Kasuya–Yoshida) model which governs the magnetic properties of the compounds based on rare earth.

The observation of an equivalent Curie temperature for the two polymorphic forms of $GdNi_3Ga_2$ is surpriing. Indeed, Gd–Gd distances are affected by the structural transition $CaCu_5$-type → $HoNi_{2.6}Ga_{2.4}$-type: in the $CaCu_5$-type (M-sample), each Gd-atom has eight nearest neighbors (2 at 0.4051 nm and 6 at 0.5086 nm), whereas in the $HoNi_{2.6}Ga_{2.4}$-type (A2-sample) the Gd species has fourteen neighbors (2 at 0.4132 nm and 12 at 0.5451 nm for the 1*a*-site (0 0 0) and 2 at 0.4132 nm, 6 at 0.5044 nm, and 6 at 0.5451 nm for the 2*d*-site (1/3 2/3 1/2)). If the average Gd–Gd distance increases, when the $HoNi_{2.6}Ga_{2.4}$-type is adopted, so does the number of neighbors.

The occurrence of an antiferromagnetic ordering in $GdNi_3Sn_2$ could be explained by the oscillatory character of the RKKY interactions versus the interatomic distances. In comparison to those existing in $GdNi_3Ga_2$ (A2-sample), the Gd–Gd distances in $GdNi_3Sn_2$ (2 at 0.4259 nm and 12 at 0.5709 nm; 2 at 0.4259 nm, 6 at 0.5297 nm, and 6 at 0.5709 nm) are much larger and cause a change of the sign of the magnetic coupling.

3.4. Hydrogen Absorption Properties of $GdNi_3Al_2$ and Their Influence on Its Magnetic Properties

After a suitable activation procedure at 573 K, as described previously in Ref. (5), the powdered M-, A1-, and A2-samples of $GdNi_3Al_2$ absorb hydrogen at room temperature under a gas pressure of 5 MPa. The maximum hydrogen concentration n_H by mol is maintained at 1.9(1) for the M- and A1-samples but at only 1.2(1) for A2. These behaviors confirm that the phases crystallizing in the $HoNi_{2.6}Ga_{2.4}$-type (approximately half of the A2-sample) have a smaller hydrogen absorption capacity. Our results agree with the recent study performed on the formation of the hydrides in the $YNi_{5-x}Al_x$ system (14). In this case, the compounds with $x = 2.5$, 2.75, and 3 which have the hexagonal $HoNi_{2.6}Ga_{2.4}$-type are inert toward hydrogen. We

note also that YNi_3Al_2, having the $CaCu_5$-type structure, absorbs 1.85 hydrogen by mol, a value close to that determined here for M- and A1-samples of $GdNi_3Al_2$.

The hydrogenated $GdNi_3Al_2$ samples were characterized by X-ray powder diffraction. The patterns of these compounds obtained from M- and A1-samples can be indexed on the basis of a hexagonal unit cell as the starting material: the lattice parameters are $a = 0.8970(2)$ nm and $c = 0.8318(2)$ nm for these hydrides. The insertion of hydrogen leads to the expansion of the unit cell volume ($V_m = 0.5796(6)\,nm^3$) by 7.3%. Two hydrides coexist after the gas treatment of the A2-sample.

The magnetization of hydrogenated M- and A1-samples increases continuously with decreasing temperature (Fig. 12). The magnetization does not tend toward saturation at low temperature as observed for starting materials (Fig. 10). We note also that the magnetization takes a lower value at the same temperature and $B = 0.025$ T: for instance, at $T = 5$ K, the magnetization of the M-sample decreases from 0.68 to 0.12 μ_B/mol after hydrogenation. No magnetic ordering can be detected from the investigation of the magnetic properties of the hydrogenated M- and A1-samples. This behavior is confirmed by the field dependence of the magnetization of hydrogenated the A1-sample (Fig. 13), which is weakly field dependent. Certainly, the spacial distribution of hydrogen in this alloy induces a distribution of the number of H-atoms surrounding each gadolinium atom; this leads to the presence of some disorder on the scale of few atomic Gd–Gd distances and favors the formation of the spin–glass states, for instance.

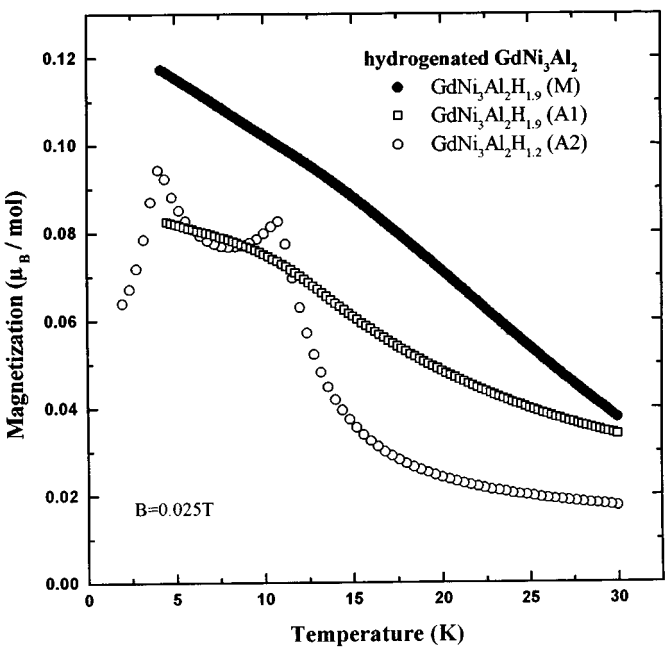

FIG. 12. Temperature dependence of the magnetization, measured with a magnetic field $B = 0.025$ T, of the three hydrogenated $GdNi_3Al_2$ samples.

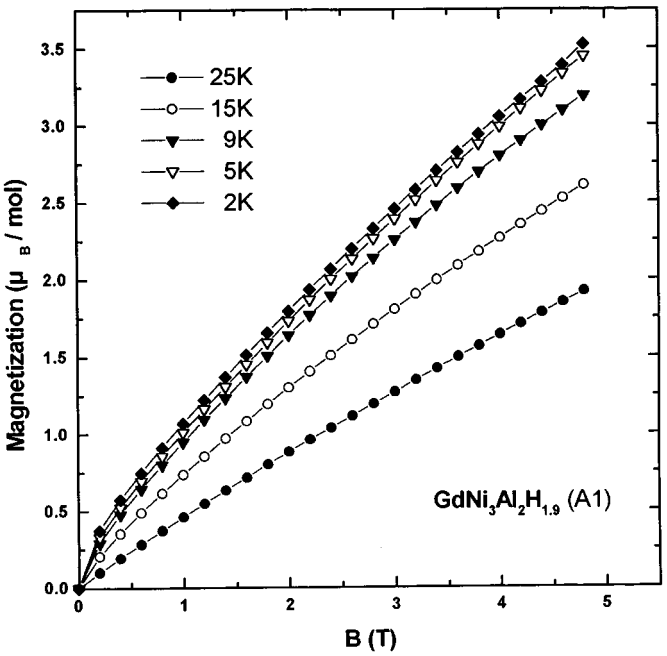

FIG. 13. Field dependence of the magnetization, measured at various temperatures, of the hydrogenated $GdNi_3Al_2$ (A1-sample).

Generally, hydrogen absorption induces a decrease of the magnetic ordering temperature of the Al-based intermetallics; e.g., the Curie temperature of $Gd_3Ni_6Al_2$ decreases from 118 to 69 K after hydrogenation (15) as does the T_C relative to GdNiAl ($T_C = 56$ K), which changes from 30 to 20 K (16–18). This behavior can be understood by considering the characteristics of the RKKY magnetic interactions: (i) the increase of Gd–Gd distances in the hydrogenated samples induces a diminution of the magnetic interactions; (ii) the insertion of hydrogen modifies the number of electrons in the conduction band of the intermetallic and changes the density of states at the Fermi level.

The influence of the hydrogen absorption on the magnetic behavior of the A2-sample can be summarized as follows (Fig. 12): the ferromagnetic transition ($T_C = 20.4(5)$ K; see Fig. 10) associated with the unknown hexagonal-phase dissapears; the magnetic transitions (T_1 and T_2) of the $HoNi_{2.6}Ga_{2.4}$-phase are unchanged. This last phase, which absorbs only a small amount of hydrogen, keeps its initial magnetic properties.

4. CONCLUSION

We have synthesized at different heat treatments the ternary intermetallics $GdNi_3X_2$ with X = Al, Ga, or Sn. The structural properties are dependent on the sample preparation procedure: $GdNi_3Sn_2$ adopts at all temperatures the

hexagonal $HoNi_{2.6}Ga_{2.4}$-type, whereas $GdNi_3Ga_2$ exhibits two hexagonal polymorphic forms having, respectively, the $CaCu_5$-type and the $HoNi_{2.6}Ga_{2.4}$-type. $GdNi_3Al_2$ presents an original behavior, adopting an unknown hexagonal structure after melting and quenching or after annealing at 1273 K. A structural determination on a single crystal is necessary in order to solve the structure of $GdNi_3Al_2$.

The nature of the X-element governs the magnetic properties of $GdNi_3X_2$ compounds. $GdNi_3Ga_2$ and $GdNi_3Al_2$ (melted sample or annealed samples at 1273 K) order ferromagnetically below 17.5(5) and 20.0(5) K, respectively. An antiferromagnetic ordering is detected below 19.5(5) K for $GdNi_3Sn_2$. This evolution from ferromagnetism to antiferromagnetism seems linked to the oscillatory character of the RKKY interactions efficient in these intermetallics.

REFERENCES

1. K. H. J. Buschow, *Rep. Prog. Phys.* **40,** 1179 (1977).
2. M. A. Fremy, D. Gignoux, J. M. Moreau, D. Paccard, and L. Paccard, *J. Less-Common Met.* **106,** 251 (1985).
3. R. V. Skolozdra, *in* "Handbook on the Physics and Chemistry of Rare Earths" (K. A. Gschneidner Jr. and L. Eyring, Eds.), Vol. 24, p. 443. Elsevier Science, North-Holland/Amsterdam/New York, 1997.
4. B. Sorgic, A. Drasner, Z. Blazina, *J. Alloys Compd.* **221,** 169 (1995).
5. J-L. Bobet, S. Pechev, B. Chevalier, and B. Darriet, *J. Alloys Compd.* **267,** 136 (1998).
6. Yu. N. Gryn, Ya. P. Yarmoluk, and V. K. Pecharsky, *Izv. Akad. Nauk SSSR Met.* **3,** 213 (1983).
7. Z. Blazina, B. Sorgic, and A. Drasner, *J. Phys. Condens. Matter* **11,** 3105 (1999).
8. JCPDS, International Centre for Diffraction Data, file number 44-1188.
9. S. R. Butler, J. E. Hanlon, and R. J. Wasilewski, *J. Phys. Chem. Solids* **30,** 1929 (1969).
10. G. F. Zhou, L. M. Di, and H. Bakker, *J. Appl. Phys.* **73,** 1521 (1993).
11. N. G. Patil, K. Glosh, and S. Ramakrishnan, *Phys. Rev. B* **52,** (1995).
12. Ch. D. Routsi, J. K. Yakinthos, and E. Gamari-Seale, *J. Magn. Magn. Mater.* **102,** 275 (1991).
13. S. Pechev, Thesis, University of Bordeaux I, no. 1935, 1998.
14. B. Sorgic, Z. Blazina, and A. Drasner, *J. Alloys Compd.* **265,** 185 (1998).
15. S. Pechev, B. Chevalier, M. Khrussanova, M. Terzieva, J-L. Bobet, B. Darriet, and P. Peshev, *J. Alloys Compd.* **259,** 24 (1997).
16. A. V. Kolomiets, L. Havela, V. A. Yartys, and A. V. Andreev, *J. Alloys Compd.* **253–254,** 343 (1997).
17. H. Drulis, W. Petrynski, and B. Stalinski, *J. Less-Common Met.* **101,** 229 (1984).
18. A. Kolomiets, L. Havela, A. V. Andreev, V. Sechovsky, and V. A. Yartys, *J. Alloys Compd.* **262–263,** 206 (1997).